Our data show that, applied to exceedingly ancient and geochemically highly altered (graphitic, carbonized) kerogenous microscopic fossils, Raman imagery can be used to correlate directly chemical composition with optically discernible morphology and to prove the presence of crucial indicators of biogenicity, such as kerogenous cell walls. When applied to particularly poorly preserved fossil-like microscopic filaments, for which optical microscopy can only hint at cellularity (Fig. 1a, c, d), this highly sensitive technique can yield convincing evidence of biogenicity. Most notably, by providing a means by which to correlate biologically characteristic (kerogenous) composition with features of morphology that typify filamentous microbes—such as cylindrical (Fig. 1a–i), sinuous (Fig. 1a, e, f, h) and tapering (Fig. 1e, f, h) filament form, and the presence of transverse cell walls (Fig. 1b, e–i) and distinctively shaped terminal cells (Fig. 1e, f, h)—optical microscopy (Fig. 1) coupled with laser–Raman imagery (Fig. 2) and measurement of Raman point spectra (Fig. 3) substantiates the biological origin of the oldest putative fossils now known (Fig. 1e–i). By the time of preservation of the diverse, exceptionally ancient, microscopic filaments of the Apex chert[4,5], ~3,500 Myr ago, microbial life was flourishing and presumably widespread. □

Methods

Optical photomicrography

We acquired the optical photomicrographs (Fig. 1) in transmitted white light with a Leitz Orthoplan 2 automatic photomicroscope.

Raman spectroscopy

Laser–Raman spectroscopic data (Figs 2 and 3) were obtained with a Dilor XY (formerly Instruments S.A., now J.Y. Horiba) 0.8-m triple-stage system that has macro-, micro- and confocal line-scan imaging options. This system permitted acquisition of both individual point spectra, typically over a period of 100 s, and true Raman images that show the spatial distribution of molecular components. The confocal capability of the system was such that we could use a 100× objective without immersion oil (having an extended working distance of 3.4 mm and a numerical aperture of 0.8) to obtain all Raman data with a planar resolution of < 1 μm and a vertical resolution of 1–3 μm. Laser wavelengths ranging from blue to infrared were provided by a coherent krypton ion laser equipped with appropriate optics. We used a wavelength of 531 nm (in the green portion of the spectrum) typically at a laser power of less than 8 mW over a 1-μm spot—an instrumental configuration that we showed to be well below the threshold that results in radiation damage to the specimens analysed.

Fossil specimens situated in the uppermost ~65 μm of petrographic thin sections were centred in the path of the laser beam projected through an Olympus BX40 microscope. The upper surfaces of thin sections were either polished (with a paste containing 1-μm-sized diamonds) or unpolished and finished by a slurry of 600 mesh carborundum. To enhance the optical image of specimens situated more than ~10 μm below the upper surface of unpolished sections, we covered the area imaged by a thin veneer (~1-μm thick) of type B non-drying microscopy immersion oil (R. P. Cargille Laboratories). Not only have appropriate analyses (see above) shown that the presence of this thin veneer has no appreciable effect on the Raman spectra acquired, but the point spectra of specimens in polished sections (for example, Fig. 1a, b) and of most specimens (12/23) analysed in unpolished sections (for examples, Fig. 1e, f, h) were obtained without this veneer.

Raman imaging

To acquire Raman images (Fig. 2), a rectangular area enclosing a part of a fossil was selected for imaging, the backscattered Raman spectra obtained in each rectangle were collected through the optical system described above along micrometre-resolution scan lines, and their x–y registrations were automatically recorded to provide a pixel-assigned array of spectral elements ('spexels')[11]. A typical Raman image comprised 25 × 25 spectral elements, each analysed for 5–10 s, resulting in a total data collection time of 50–100 min for each image. We processed the several hundred spexels for each specimen by constructing a map of the intensity in the spectral window corresponding either to the 'D' band (at ~1,350 cm^{-1}) or the 'G' band (~1,600 cm^{-1}) of the kerogenous material; maps made by the 'G' band were generally of relatively higher Raman image quality. The resulting 'chemical image' shows the areal distribution of the fossil structures that produced the Raman spectral bands originating from specific molecular components.

Received 3 July; accepted 30 November 2001.

1. Schopf, J. W. in *The Proterozoic Biosphere, A Multidisciplinary Study* (eds Schopf, J. W. & Klein, C.) 587–593 (Cambridge Univ. Press, New York, 1992).
2. Schopf, J. W. & Walter, M. R. in *Earth's Earliest Biosphere, Its Origin and Evolution* (ed. Schopf, J. W.) 214–239 (Princeton Univ. Press, Princeton, 1983).
3. Mendelson, C. V. & Schopf, J. W. in *The Proterozoic Biosphere, A Multidisciplinary Study* (eds Schopf, J. W. & Klein, C.) 865–951 (Cambridge Univ. Press, New York, 1992).
4. Schopf, J. W. in *The Proterozoic Biosphere, A Multidisciplinary Study* (eds Schopf, J. W. & Klein, C.) 25–39 (Cambridge Univ. Press, New York, 1992).
5. Schopf, J. W. Microfossils of the Early Archean Apex chert: new evidence of the antiquity of life. *Science* **260,** 640–646 (1993).
6. Buick, R. Carbonaceous filaments from North Pole, Western Australia: are they fossil bacteria in Archean stromatolites? *Precambrian Res.* **24,** 157–172 (1984).
7. Awramik, S. M., Schopf, J. W. & Walter, M. R. Carbonaceous filaments from North Pole, Western Australia: are they fossil bacteria in Archean stromatolites? A discussion. *Precambrian Res.* **39,** 303–309 (1988).
8. Buick, R. Carbonaceous filaments from North Pole, Western Australia: are they fossil bacteria in Archean stromatolites? A reply. *Precambrian Res.* **39,** 311–317 (1988).
9. Hayes, J. M., Des Marais, D. J., Lambert, I. B., Strauss, H. & Summons, R. E. in *The Proterozoic Biosphere, A Multidisciplinary Study* (ed. Schopf, J. W. & Klein, C.) 81–134 (Cambridge Univ. Press, New York, 1992).
10. House, C. H. *et al.* Carbon isotopic composition of individual Precambrian microfossils. *Geology* **28,** 707–710 (2000).
11. Kudryavtsev, A. B., Schopf, J. W., Agresti, D. G. & Wdowiak, T. J. *In situ* laser–Raman imagery of Precambrian microscopic fossils. *Proc. Natl Acad. Sci. USA* **98,** 823–826 (2001).
12. Schopf, J. W. & Fairchild, T. R. Late Precambrian microfossils: a new stromatolitic microbiota from Boorthanna, South Australia. *Nature* **242,** 537–538 (1973).
13. Barghoorn, E. S. & Tyler, S. A. Microorganisms from the Gunflint chert. *Science* **147,** 563–577 (1965).
14. Walsh, M. M. & Lowe, D. R. Filamentous microfossils from the 3,500-Myr-old Onverwacht Group, Barberton Mountain Land, South Africa. *Nature* **314,** 530–532 (1985).
15. Schopf, J. W. & Packer, B. M. Early Archean (3.3-billion to 3.5-billion-year-old) microfossils from Warrawoona Group, Australia. *Science* **237,** 70–73 (1987).
16. Tuinstra, F. & Koenig, J. L. Raman spectra of graphite. *J. Chem. Phys.* **53,** 1126–1130 (1970).
17. Williams, K. P. J., Nelson, J. & Dyer, S. *The Renishaw Raman Database of Gemological and Mineralogical Materials.* (Renishaw Tranducers Systems Division, Gloucestershire, England, 1997).
18. McMillan, P. F. & Hofmeister, A. M. Infrared and Raman spectroscopy. *Rev. Mineral.* **18,** 99–159 (1988).

Acknowledgements

We thank M. Walsh for loan of the Kromberg specimens; The Natural History Museum, London, for loan of the Apex specimens; and J. Shen-Miller for manuscript review. This work was supported by grants from the JPL/CalTech Astrobiology Center (to J.W.S.) and from the National Aeronautics and Space Administration Exobiology Program (to T.J.W.). A.D.C. is an NSF predoctoral Fellow. The Raman imaging facility at the University of Alabama at Birmingham is a consequence of the vision of L. DeLucas.

Correspondence and requests for materials should be addressed to J.W.S. (e-mail: schopf@ess.ucla.edu).

Questioning the evidence for Earth's oldest fossils

Martin D. Brasier*, Owen R. Green*, Andrew P. Jephcoat*, Annette K. Kleppe*, Martin J. Van Kranendonk†, John F. Lindsay‡, Andrew Steele§ & Nathalie V. Grassineau‖

* *Earth Sciences Department, University of Oxford, Parks Road, Oxford OX1 3PR, UK*
† *Geological Survey of Western Australia, 100 Plain Street, East Perth, Western Australia, 6004, Australia*
‡ *Research School of Earth Sciences, Australian National University, Canberra ACT 0200, Australia*
§ *School of Earth, Environmental and Physical Sciences, University of Portsmouth, Burnaby Road, Portsmouth PO1 3QL, UK*
‖ *Department of Geology, Royal Holloway University of London, Egham Hill, Surrey TW20 0EX, UK*

Structures resembling remarkably preserved bacterial and cyanobacterial microfossils from ~3,465-million-year-old Apex cherts of the Warrawoona Group in Western Australia[1–4] currently provide the oldest morphological evidence for life on Earth and have been taken to support an early beginning for oxygen-producing photosynthesis[5]. Eleven species of filamentous prokaryote, distinguished by shape and geometry, have been put forward as meeting the criteria required of authentic Archaean micro-

fossils[1–5], and contrast with other microfossils dismissed as either unreliable or unreproducible[1,3,6,7]. These structures are nearly a billion years older than putative cyanobacterial biomarkers[8], genomic arguments for cyanobacteria[9], an oxygenic atmosphere[10] and any comparably diverse suite of microfossils[5]. Here we report new research on the type and re-collected material, involving mapping, optical and electron microscopy, digital image analysis, micro-Raman spectroscopy and other geochemical techniques. We reinterpret the purported microfossil-like structure as secondary artefacts formed from amorphous graphite within multiple generations of metalliferous hydrothermal vein chert and volcanic glass. Although there is no support for primary biological morphology, a Fischer–Tropsch-type synthesis of carbon compounds and carbon isotopic fractionation is inferred for one of the oldest known hydrothermal systems on Earth.

The Apex microfossils were reported to occur in rounded grains of chert (microcrystalline silica) transported a great distance before redeposition in a bedded grainstone conglomerate[2,3,5], in a setting compared with a wave-washed beach or the mouth of a stream or river[5]. However, recent field mapping and sampling (Fig. 1) reveals that the fossiliferous chert at Chinaman Creek is not part of the bedded succession. It is a breccia that infills one of a series of chert veins (Fig. 1, sample 4) that cross-cuts pillow basalts and feeds up into, and is continuous with, overlying stratiform cherts (Fig. 1, samples 6–8)[11]. Textural and scanning electron microscope–energy dispersive X-ray (SEM–EDX) studies indicate a suite of hydrothermally associated minerals plus the hydrothermal alteration of adjacent pillow basalts but not overlying komatiitic basalts (Fig. 1; see Methods). A hydrothermal origin is inferred for this vein and closely associated stratiform cherts, much like that inferred for some barite-chert beds of the 3,490 million year (Myr) Dresser Formation at nearby North Pole[12].

We find no evidence for surface sedimentary structures or textures (for example, sorting or rounded quartz) in the microfossiliferous clasts. Petrography of both figured and re-collected microfossiliferous chert samples (Fig. 1, sample 4) from the chert breccia vein reveals multiple generations of fissure filling (fabric A, generations A1 to A4), brecciation, and veining by chalcedonic microquartz (fabric B1 to B3), with a final phase of void-filling by megaquartz (fabric C; Fig. 1; see Methods and Supplementary

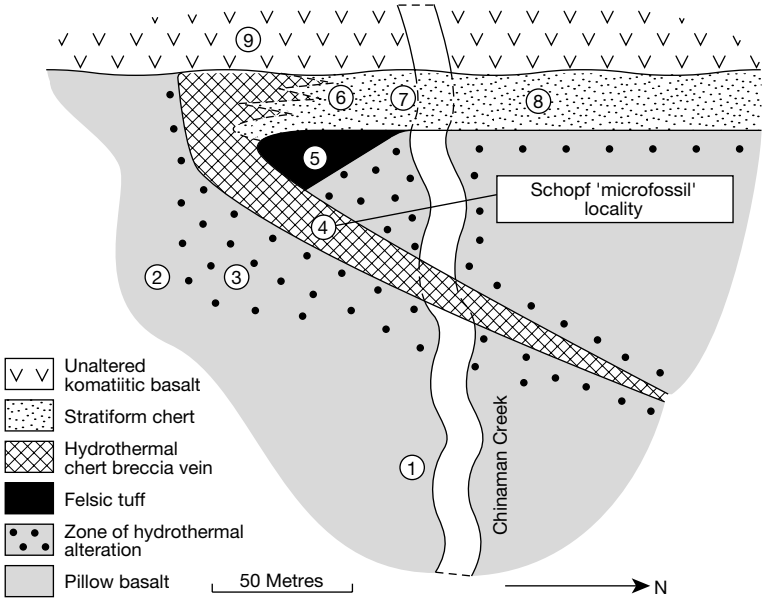

	1	2	3	4 A1/B1	4 A2/B2	4 A3/B3	4 C/A4	5	6	7	8	9
Chromite	–	–	–	●	●	■	–	● ■	–	–	–	–
Iron oxide	■	■ □	■	●	●	● ■	–	● ■	■	–	–	■ □
TiO_2	■	■	–	●	● ■	● ■	–	● ■ □	–	–	■	■ □
$BaSO_4$	–	□	–	● ■	● ■	● ■	■ □	■ ○ □	● ■	■ ○	■ ○	–
Alunite–jarosite	–	–	–	● ■	● ■	● ■	■ □	–	■ ⋆	● ■ ⋆	● ○ ■ ⋆	–
Aluminosilicates	■	■	■	● ■	● ■	● ■	–	● ○ ■	–	–	–	■ □
Metals, *sulphides*	*Cu* ■	Ni □ Cu □ Zn □ Pb □	–	Fe ● Ni ● Cu ● Zn ● *Pb* ●	Fe ● ■ *Fe* ● ■ Ni ● Cu ● Zn ● Sn ● *Pb* ●	Fe ■ *Fe* ■ Cu ●	*Pb* □	Pb ●	*Fe* ■ *Cu* ■ Zn ■	*Fe* ● ■ *Ni,As* □ *Cu* ● ■ *Cu* ○ □	Fe ■ *Fe* ● ○ *Cu* ■ *Zn* ● ○ *Zn* ■ □ *Sb* ● ○ *Sb* ■ □	–
Sulphur (p.p.m.)				–	162	79			–	330	607	
Graphite				● ■	● ■	● ■		● ○ ■	●	●	● ○ ■	
Carbon (p.p.m.)				126–1206	1413	36			34	2545	2162	
$\delta^{13}C_{PDB}$ (‰)				–30.3 –26.5	–29.9	–28.4			–25.6	–29.5	–25.6	
$\delta^{18}O_{SMOW}$ (‰)				+14.5 +14.7	+14.5	+14.6 +14.7			+14.3	+14.1	+13.7	

● In shards, clasts ○ Around shards, clasts ■ In matrix □ In veins ⋆ Arsenic-rich
A-C, Fabrics recognized in thin section Open box, not analysed

Figure 1 Geological sketch map of the Apex chert at Chinaman Creek, showing sample numbers and site of the Schopf 'microfossil' locality (sample 4) from a metalliferous hydrothermal chert breccia vein that cross-cuts hydrothermally altered pillow basalt. Samples 1–9 are from this study. New geochemical data are consistent with a hydrothermal setting (see Methods).

Information Fig. 1a, b). Structures with undulose laminations (Supplementary Information Fig. 1a, S) have hitherto been regarded as stromatolite-like clasts[3]. However, we find that they can show intimate relationships with enclosing fabrics of A1–A3, forming void-filling drapes and overhangs. These 'stromatoloids' contain lithoclasts, phyllosilicates, metallic oxides, sulphides and rhombic ghosts like those of the enclosing fabric. We reinterpret these stromatoloids as isopachous internal cements of generations B1–B3.

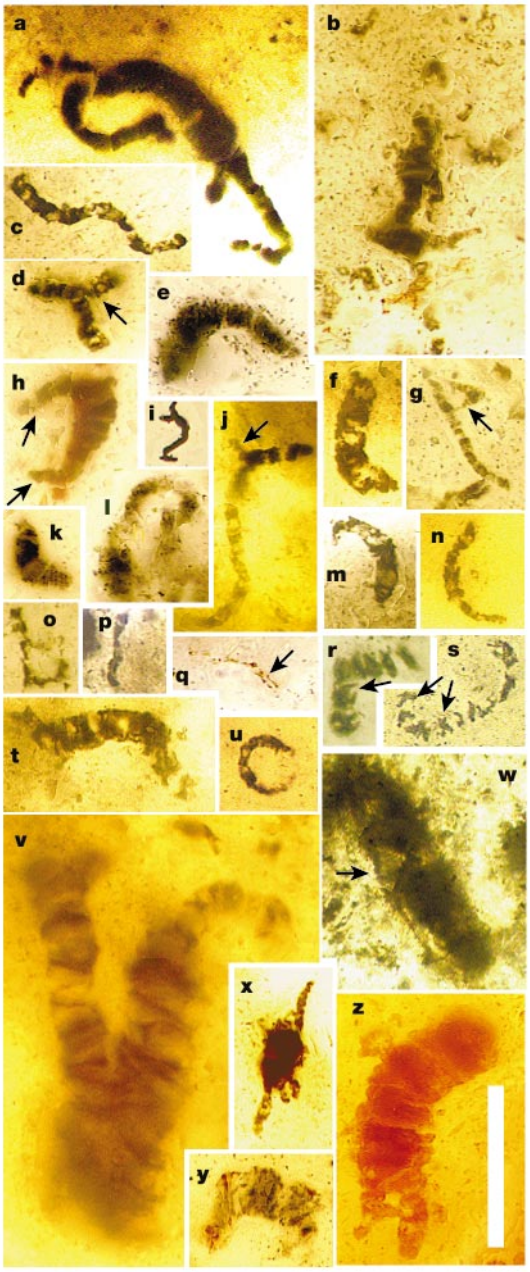

Figure 2 Automontages of inferred artefacts from the Apex chert. **a**, **b**, **o**, **u**, **v**, **x**, Pseudoseptate and branched filamentous artefacts from vein chert (NHM V.63127, 63164, 63165, 63127, 63164, 63164). **i**, Artificial graphite filament (63166). **e**, **k**, **l**, Filamentous artefacts from felsic tuff (**e** and **k** from chalcedony matrix; **l** from within devitrified rim of volcanic glass shard). **p**, Pseudoseptate filament from clast in stratiform chert. **c**, **d**, **f**–**h**, **j**, **m**, **n**, **q**–**t**, **w**, **y**, **z**, New images of previously illustrated structures (refs 2, 3; holotypes*): **c**, *Primaevifilum amoenum*; **d**, *A. disciformis*; **f**, *P. laticellulosum**; **g**, *P. delicatulum**; **h**, *P. attenuatum**; **j**, *P. amoenum**; **m**, *P. conicoterminatum**; **n**, type C narrow filament; **q**, *Archaeotrichion septatum**; **r**, **s**, 'trichome showing bifurcated cells'; **t**, type A broad filament; **w**, cf. *A. grandis**; **y**, 'type B' broad filament; **z**, *Archaeoscillatoriopsis maxima**. Bright-field transmitted light. Scale bar, 40 μm; arrows indicate anomalies (see the text).

High-resolution stable isotopic analyses of fabrics from freshly cut rock slices reveal a range of $\delta^{13}C_{PDB}$ values (where $\delta^{13}C = [(^{13}C/^{12}C)_{sample}/(^{13}C/^{12}C)_{standard}] - 1$) of −30‰ to −26‰ for reduced carbon (see Methods and Fig. 1), which is comparable with results from earlier studies and not inconsistent with biogenic fractionation[4,13]. Of these, the most negative $\delta^{13}C$ value is likely to be the best preserved, as indicated by dehydrogenation studies of Warrawoona kerogens elsewhere[4]. Our values of −30‰ are in the range of those obtained from other early hydrothermal cherts[14]. Oxygen isotopes for SiO_2 of +13.7‰ to +14.7‰ are less ^{18}O-enriched than many Archaean sedimentary cherts (compare ref. 15). Along with native metals (Fe, Ni, Cu, Zn, Sn) (Fig. 1), this suggests that comparatively high (~250–350 °C) hydrothermal temperatures were reached[15]. The relatively high sulphur concentrations found within the stratiform cherts (330–607 p.p.m.) (Fig. 1) are shown by EDX to lie within rhombic pseudomorphs of microcrystalline quartz after sulphate or within microscopic sulphide grains that have complexly intergrown barite, alunite and jarosite (often arsenic-rich). Sulphur isotopic values of −6 to +5‰ $\delta^{34}S_{CDT}$ (Fig. 1) from combined sulphide–sulphate microsamples in these stratiform cherts are close to those obtained from broadly coeval sulphides and barite at the nearby North Pole, where sulphate growth resulted either from the hydrothermal alteration of evaporitic gypsum and anhydrite[16] or from the reactions involving exhalative sulphur species in near-surface conditions[11,12].

Much of the fossil-bearing rock within the chert was reported to consist of rounded clasts and lithic fragments, of which about 5% were suggested to comprise a petrographically distinctive population yielding microfossils said to be absent from all other clasts and the surrounding matrix[2,3]. This was interpreted to indicate that these clasts were initially preserved in an older unit, some part of which was eroded, transported and redeposited as a detrital component of the bedded chert[2,3]. Our findings give no support to this interpretation. The figured microfossil-like structures occur in rounded to angular clasts of early fabric A1 (~40%), within second or later generations of fissure filling (A2, A3; ~57%) and in later, metastable chert matrix (B3; ~3%; see Supplementary Information Table 1), calling their primary origin into question. Comparable graphitic structures also occur in both clasts and matrix of the stratiform cherts (Fig. 2p), within glass rims of volcanic shards (Fig. 2l) and in the associated chalcedony matrix of the felsic tuffs (Fig. 2e, k), clearly calling their biogenicity into question.

The structures thought to be cellularly permineralized microfossils[1–3] occur mainly as isolated, irregularly distributed and randomly orientated filaments in these fabrics. They therefore differ from typical populations of Proterozoic to modern cyanobacteria, in which the trichomes commonly occur clustered together in layers, often with a distinctive orientation relative to bedding (for example, ref. 17). Previous authors[1–3] have interpreted the darker mineral of these filaments to be kerogen and the transecting paler areas to be of cellular origin, taken together to reflect a trichomic organization like that of Proterozoic to modern bacteria and cyanobacteria. Features interpreted as the terminal and medial cell shape, the cellular dimension and the degree of trichomic attenuation have then been used to distinguish 11 taxa of filamentous microfossils[2,3].

We have made detailed, digital automontage images of the figured material of purported microfossils (including holotypes and paratypes) and of associated, previously unillustrated filamentous microstructures (Figs 2 and 3; see Methods). A few of the filaments are sinuous and S-shaped (for example, Fig. 2c, j) but most are tightly C- or J-shaped (for example, Fig. 2m, z) or L-shaped (for example, Fig. 2r) and some are almost completely closed planar

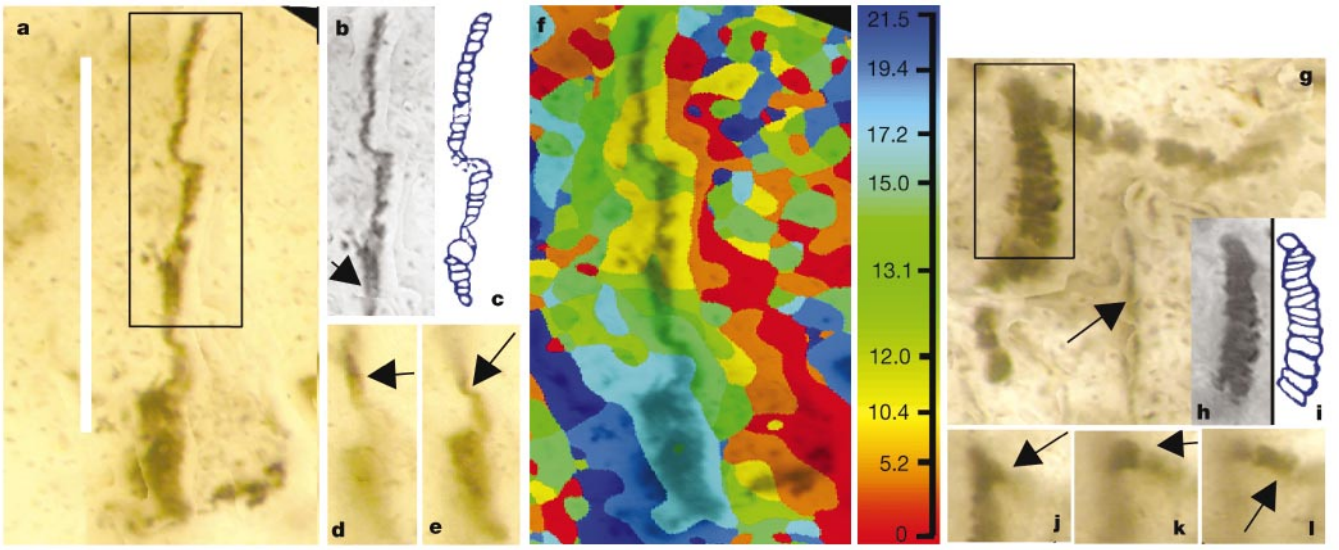

Figure 3 Automontages of inferred artefacts from the Apex chert. **a**, New image of putative beggiatoan *Eoleptonema apex* Holotype (ref. 3), combining the most sharply focused images from successive focal planes; **b**, **c**, digital image and interpretative sketch in the style of ref. 3 that omits the lower structure; **d**, **e**, new single image frames showing continuity of original and newly imaged structures. **f**, Topographic map showing computer-selected focal planes (plus scale in μm) of **a**; **g**, new image of putative cyanobacterium *Archaeoscillatoriopsis disciformis* Holotype (ref. 3) showing rhombic ghost (arrow); **h**, **i**, digital image and interpretative sketch in the style of ref. 3 that omits the lower structure and side branch; **j**, **k**, **l**, new single image frames showing continuity of original and newly imaged structure. Scale bar, 40 μm.

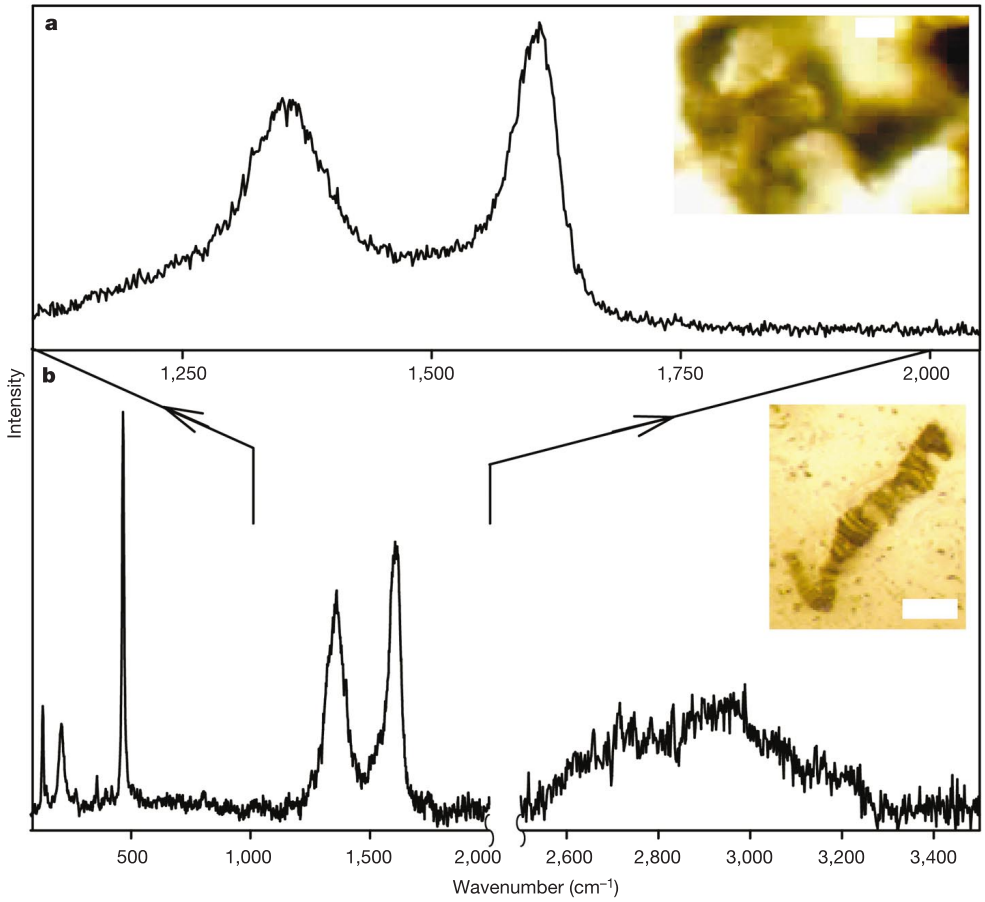

Figure 4 Raman spectra of associated graphitic objects (<1 mm apart) within NHM V.63165. **a**, Spherulitic mass in B2; **b**, pseudofossil identified as a 'degraded cellular filament or wrinkled sheath' (Fig. 1.5.4B in ref. 2) within fabric A1, showing quartz modes (128, 206, 355 and 464 cm^{-1}) plus first- and second-order graphitic carbon peaks. Comparable spectra are also produced by dark microclasts within fabric A2 and dendritic pseudoseptate mullions within fabric B2. Background has been subtracted. Scale bar for insets, 10 μm.

circles (Fig. 2u). Many of the filamentous structures are branched or formed in ways not shown in the original descriptions and illustrations[1–3] because of the choice of focal depth and/or illustrated field of view. In *Primaevifilum amoenum*, interpreted as a prokaryote cellular trichome (ref. 2), the holotype, found within fabric A2, is seen to have a small continuous side branch (Fig. 2j). In *Archaeoscillatoriopsis disciformis* of inferred oscillatoriacean cyanobacterial affinity[3], the holotype (Fig. 3g–l) is seen to be part of a continuous bifurcating structure within fabric A3 whose shape closely follows that of a nearby rhombic crystal ghost (Fig. 3g, arrow). In *P. delicatulum*, compared with modern Oscillatoriacea[2], the holotype is found to be part of a complex structure involving a continuous upper side branch (Fig. 2g). Branching is inconsistent with an oscillatoriacean affinity and not generally confirmed in the fossil record until ~900–800 Myr (ref. 18). We also find a continuum between such filaments and numerous comparable but unreported pseudoseptate artefacts with multiple, chaotic branches of markedly varying diameters (Fig. 2a, b) and multiple filaments radiating from a bulbous central body (Fig. 2x) that occur nearby in the type slides.

The holotype of *Eoleptonema apex*, compared with the modern bacterium *Beggiatoa*[3], is found to be part of a larger, sharply angular structure (Fig. 3a–f) that we infer to have formed around rhombic crystal ghosts within fabric A2, much as in Fig. 2o. The tiny thread-like holotype in *Archaeotrichion septatum* (Fig. 2q) is seen to be part of a larger branched structure, deflected along planes between quartz crystals, in an area of pervasive iron staining within fabric B3. One end of the holotype of *Primaevifilum attenuatum* was originally reconstructed (Fig. 5G in ref. 3) to incorporate a contiguous iron-stained fracture; the newly montaged structure is strongly arcuate (Fig. 2h) and lies within fabric A2. A further observation concerns maximum filament width, which was much greater (19.5 μm) than seen in most other Precambrian microfossil assemblages[3]. Our studies extend this phenomenon, revealing branched pseudoseptate structures up to 36 μm in diameter (Fig. 2v).

High-resolution Raman spectroscopy has been suggested as a technique that can clarify the carbonaceous nature of an ancient microfossil-like object of putative but uncertain biogenicity, especially if it lies too far beneath the surface for other surface analytical techniques[19]. Biogenicity would remain unproved, however, if associated artefacts and the groundmass were of the same composition and particle size as the filaments. That is what we find in this case. In Fig. 4 we compare high-resolution micro-Raman spectra of a figured microfossil in fabric A1 with that of an associated spherulitic artefact in fabric B2. Both show Raman modes from a matrix of microquartz (diameter 5–10 μm) plus a multiplet at 1,356 and 1,606 cm^{-1} and weaker bands at around 2,710 and 2,935 cm^{-1} (Fig. 4b) characteristic of first-order and second-order bands of amorphous graphite[20], respectively. The mode intensities increase in direct relation to the strength of apparent black coloration observed in transmitted light. Unlike concentrated samples of carbon, such as kerogen and coal, there is little direct absorption of the incident laser power, even for much higher powers than were used to collect these spectra, suggesting that the graphite is dilute and thermally protected by the bulk (quartz) host phase. The relative mode intensities[20,21] indicate a graphite particle size of ~200 nm for groundmass, artefacts and 'filaments' alike.

Most of these filamentous structures were claimed to preserve traces of septa which, in each filament, were thought to maintain a shape and size consistent with a biological origin[2,3]. However, micro-Raman and thin-section petrography suggest that the septate appearance of the filaments is largely created by microcrystalline quartz grains (~1–10 μm) interspersed with darker amorphous graphite that makes up the bulk of the filament (for example, Fig. 2f, g). The appearance of numerous thin septa seems to be caused by more closely packed plates of graphite and is even seen in micro-fossil-like structures within volcanic glass (Fig. 2e, k). The impression of supposed 'bifurcated cells' or 'cell pairs' in the process of division[2,3] (Fig. 2r, s, arrows) can be explained by irregular alternations of darker, platy graphite with paler quartz. The illusion of septation is weakest in those cases in which the filament is thicker and the quartz grains are more randomly scattered through the graphite (Fig. 2d, t). In the presumed holotype of *A. grandis*, the crudely septate appearance can be explained by rhombic crystal ghosts (for example, Fig. 2w). Chains of tiny cell-like blobs in the holotype of *Archaeotrichion septatum* (Fig. 2q) are here interpreted as small mineral grains trapped between the planar interfaces of quartz crystals.

Ancient filamentous structures should not be accepted as being of biological origin until all possibilities of their non-biological origin have been exhausted. In particular, it is important to note that complex 'septate' carbonaceous structures can result from experimental hydrothermal processes[22,23]. Our study of the Apex chert microfossils reveals that most are part of a morphological continuum (a 'symmetry-breaking cascade') ranging from spheroidal through bulbous, radiating and chaotically branching to arcuate forms (compare refs 7 and 22). 'Holotypes' often lie close to patches of spherulitic or botryoidal (hemispherical) chalcedony with graphitic rims of identical mineralogical appearances, compositions and particle sizes in micro-Raman spectra (see Supplementary Information Table 1). Where concentrations of graphitic impurities are high, we find that secondary spherulites of silica (formed by the crystallization of glassy or colloidal silica to fibrous chalcedonic quartz) are surrounded by nearly spherical masses of graphite, producing a spongy, spheroidal fabric in thin section (for example, Fig. 4a; Supplementary Information Fig. 1c, M1). In layers where graphitic impurities are fewer, thinner dendritic to arcuate mullions of graphite separate the spherulites (compare Fig. 2a, b, d; Supplementary Information Fig. 1c, M2). In more distal regions of purer chalcedony, the localized impurities tend to be concentrated into filamentous arcuate mullions of graphite (for example, Fig. 2c–f; Supplementary Information Fig. 1c, M3). These reaction rims can have a pseudoseptate appearance owing to the contraction and microfracturing of the amorphous graphite or to the presence of small grains or radiating sheets of quartz. We attribute variations in filament size and shape to localized variations in primary texture and spherulite and botryoid size and shape. We find that similar (but non-septate) filamentous pseudofossils are mimicked by pencil graphite infilling the arcuate fractures around chalcedony spherulites and botryoids near figured specimens (Fig. 2i). Of the 11 holotypes of prokaryotic 'microfossils' defined from these rocks[2,3], we regard those of *E. apex* (Fig. 3a–f) and *A. septatum* (Fig. 2q) to be mineral rims that formed around crystal margins, whereas the others can be explained as arcuate, sinuous and branched mineral rims of spherulitic origin.

Reinterpretation of the Warrawoona structures as artefacts raises serious questions about the presence of cyanobacteria at 3,460 Myr, especially because the biogenic origin of many broadly coeval stromatolites[24] and the evolutionary context[9,10] could be regarded as moot[24]. Instead, we find evidence consistent with a hydrothermal setting for the Apex chert at Chinaman Creek. Carbon isotopic values from the graphitic cherts imply a significant biological contribution to the carbon cycle, perhaps from otherwise unpreserved hyperthermophile bacteria like those thought to occur as microfossils in younger Archaean rocks[25]. That would be consistent with evidence from the sequencing of bacterial ribosomal RNA, which indicates that methanogenic archaebacteria are arguably of much greater antiquity than cyanobacteria[9]. However, the estimated temperatures (~250–350 °C) imply a much more extreme hydrothermal habitat than currently occupied. We suggest that redox buffers (for example, native metals within the graphitic vein cherts) could have encouraged the transformation of volcanogenic CO into isotopically light carbon compounds via a Fischer–Tropsch-type

synthesis[26,27], which would fit well with a hydrothermal cradle for early life. □

Methods

Field mapping, petrography, SEM–EDX

Tholeiitic pillow basalts adjacent to the vein (Fig. 1, samples 2 and 3) are bleached by the effects of hydrothermal alteration and fissured by numerous small barite-rich and metalliferous chalcedonic quartz veins, like those in the main breccia vein. Pillow basalts away from the vein (Fig. 1, sample 1) as well as komatiitic basalts above the bedded chert (Fig. 1, sample 9) are less affected by hydrothermal alteration. A wedge of felsic tuff with devitrified glass shards occurs near the top of the dyke (Fig. 1, sample 5) and is interpreted as an initial volcanic eruption from the fissure now occupied by the chert breccia vein. Similar felsic tuffaceous material has been silicified within the stratiform chert (Fig. 1, sample 6).

Optical petrography was performed on re-collected material with the use of 30-μm, 150-μm and 240-μm sections. Polished slices, hydrofluoric acid (HF)-etched rock chips and HF residues were examined under Jeol-840A and Phillips XLS30S field-emission SEMs, fitted with a light-element EDX system operating at 1–15 kV. EDX analysis shows that barite ($BaSO_4$) is common in both vein and stratiform cherts, together with other hydrothermally associated minerals: native metals, sulphides, chalcedonic quartz and megaquartz (Fig. 1). Both vein chert and felsic tuff contain grains of chromite ($FeCr_2O_4$), iron oxide and TiO_2 (for example, relicts from hydrothermal leaching or fracturing of adjacent mafic extrusives) plus Al- and K-rich phyllosilicates from hydrothermally altered feldspars. The black stratiform cherts (Fig. 1, samples 6–8) comprise weakly bedded packstones or grainstones characterized by alunite-like and jarosite-like sulphates rich in Al, K, Fe and As (for example, from hydrothermal reactions involving sulphuric acid, feldspars, zeolites or sulphides). Bedding is overprinted near the vein by rhombs, now of chalcedonic quartz, containing relict grains of barite and alunite, which are indicative of oversaturated brines near a hydrothermal vent.

Fabric mapping, automontage

Generation A1 of the vein chert (Fig. 1, sample 4) comprises brecciated, angular to rounded fragments of microcrystalline quartz containing graphitic microclasts, grains of iron oxide, rutile, chromite, native metals (Fe, Ni, Cu, Zn, including beside 'holotypes'), pyrite, sericite and rhombic pseudomorphs. The latter include relict grains of barite, plus dark reaction rims of chromite and rutile (under EDX) and amorphous graphite (in micro-Raman spectra; see below). A1 clasts are commonly traversed by small cracks and vugs now of chalcedonic microquartz (fabric B1), possibly replacing massive nodular sulphate or infilling voids left by their dissolution. A1 fragments were further brecciated by successive episodes of fracturing *in situ*, so that adjacent clasts often have a 'jigsaw puzzle' fit. The cavities thus formed were lined with epitaxial rims of spherulitic and fan-shaped white chalcedonic microquartz (fabric B2). Fissure-filling chert of generation A2 (paler with more distinct lithoclasts) was produced by fracturing and spalling of A1 and B1, geopetally infilling voids within the breccia (Supplementary Information Fig. 1a). A comparable process led to generations A3 and B3 (Supplementary Information Fig. 1b). Conspicuous rhombic crystals (barite in EDX) or voids float in the outer margins of cross-cutting B3, which penetrates clasts of A1 and A2 via small fissures and vugs, forming laminated layers (Supplementary Information Fig. 1a) and botryoids. Each phase was accompanied by carbonaceous (hydrocarbon?) migration, penetrating along microfissures to line or infill small vugs within A1, coat and darken clasts of A1–A3 and B1–B2, and accumulate within botryoidal–spherulitic cherts of B2–B3. The central zone of wider chalcedonic veins was later infilled by crystals of drusy quartz, largely lacking in graphite (Supplementary Information Fig. 1a, b: C). Late-stage metallic oxides, often associated with secondary oxidation and reddening, infiltrate small cracks and fissures. Neither Raman nor SEM–EDX studies revealed the presence of carbonate.

Rock slices were examined under bright-field transmitted and reflected light with Nikon Optiophot-2 (biological) and Optiophot-pol (polarizing) microscopes, imaged with a single-chip RGB camera and processed with Acquis-Pro and Automontage image-capturing software. Automontage captures a succession of still digital images of three-dimensional structures at successive focal planes (Fig. 3), combining the most-sharply focused images into a single montage (Fig. 3a, g), showing the planes used (Fig. 3f).

Micro-Raman spectroscopy and stable isotopes

Micro-Raman spectroscopy, with spatial-filtering confocal aperture, was performed on rock slices, polished thin sections and type slides. Raman spectra were recorded in both 135° scattering and 180° backscattering geometry with a SPEX Triplemate equipped with a back-illuminated, liquid-N_2-cooled charge-coupled-device detector. Spectra were excited by the 488.1-nm and 514.5-nm lines of an Ar^+ laser, focused down to a 1–5-μm spot on the sample, with powers of ~10–30 mW. This power range is well below the thermal-damage threshold from local heating by the laser beam and below the threshold for any laser-induced downshift in the measured vibrational frequencies[28]. Carbon and sulphur isotopes and concentrations (mostly replicate) were obtained from coarsely crushed, hand-picked samples of re-collected material and analysed with a He continuous-flow isotope ratio mass spectrometer[29] consisting of an elemental analyser Carbo Erba EA 1500 on line to an Optima mass spectrometer. Oxygen isotopes were obtained with a Synrad CO_2 laser–BrF_5 fluorination automatic system on line to an Optima mass spectrometer (method adapted from ref. 30).

Received 14 February 2001; accepted 24 January 2002.

1. Schopf, J. W. & Packer, B. M. Early Archean (3.3 billion to 3.5 billion-year-old) microfossils from Warrawoona Group, Australia. *Science* **237,** 70–73 (1987).
2. Schopf, J. W. in *The Proterozoic Biosphere: a Multidisciplinary Study* (eds Schopf, J. W. & Klein, C.) 25–39 (Cambridge University Press, Cambridge, 1992).
3. Schopf, J. W. Microfossils of the Early Archean Apex Chert: new evidence of the antiquity of life. *Science* **260,** 640–646 (1993).
4. Schopf, J. W. in *Early Life on Earth* (ed. Bengtson, S.) 193–206 (Columbia University Press, New York, 1994).
5. Schopf, J. W. *The Cradle of Life* (Princeton Univ. Press, New York, 1999).
6. Buick, R., Dunlop, J. S. R. & Groves, D. I. Stromatolite recognition in ancient rocks: an appraisal of irregularly laminated structures in an early Archaean chert-barite unit from North Pole, Western Australia. *Alcheringa* **5,** 161–181 (1981).
7. Buick, R. Microfossil recognition in Archean rocks: an appraisal of spheroids and filaments from a 3500 M.Y. old chert-barite unit at North Pole, Western Australia. *Palaios* **5,** 441–459 (1990).
8. Summons, R. E., Jahnke, L. L., Hope, M. & Logan, G. A. 2-Methylhopanoids as biomarkers for cyanobacterial oxygenic photosynthesis. *Nature* **400,** 554–557 (1999).
9. Hedges, S. B. *et al.* A genomic timescale for the origin of eukaryotes. *BioMed Central Evol. Biol.* **1,** article 4, 1–10 (2001).
10. Catling, D., Zahnle, K. J. & McKay, C. P. 2001. Biogenic methane, hydrogen escape, and the irreversible oxidation of early Earth. *Science* **293,** 839–843 (2001).
11. Van Kranendonk, M. J. Volcanic degassing, hydrothermal circulation and the flourishing of life on Earth: new evidence from the c. 3.45 Ga Warrawoona Group, Pilbara Craton, Western Australia. *Precambrian Res.* (in press).
12. Nijman, W., De Bruin, K. & Valkering, M. Growth fault control of early Archaean cherts, barite mounds, and chert-barite veins, North Pole Dome, Eastern Pilbara, Western Australia. *Precambr. Res.* **88,** 25–52 (1998).
13. Strauss, H. & Moore, T. B. in *The Proterozoic Biosphere: a Multidisciplinary Study* (eds Schopf, J. W. & Klein, C.) 711–798 (Cambridge University Press, Cambridge, 1992).
14. de Ronde, C. E. J. & Ebbesen, T. W. 3.2 b.y. of organic compound formation near sea-floor hot springs. *Geology* **24,** 791–794 (1996).
15. Robert, F. Carbon and oxygen isotope variations in Precambrian cherts. *Geochim. Cosmochim. Acta* **52,** 1473–1478 (1988).
16. Shen, Y., Buick, R. & Canfield, D. E. Isotopic evidence for microbial sulphate reduction in the early Archaean era. *Nature* **410,** 77–81 (2001).
17. Awramik, S. M. & Semikhatov, M. A. The relationship between morphology, microstructure, and microbiota in three vertically intergrading stromatolites from the Gunflint Iron Formation. *Can. J. Earth Sci.* **16,** 484–495 (1979).
18. Mendelson, C. V. & Schopf, J. W. in *The Proterozoic Biosphere: a Multidisciplinary Study* (eds Schopf, J. W. & Klein, C.) 867–951 (Cambridge University Press, Cambridge, 1992).
19. Kudryatsev, A. B., Schopf, J. W., Agresti, D. G. & Wdowiak, T. J. In situ laser-raman imagery of Precambrian microscopic fossils. *Proc. N. Am. Acad. Sci.* **98,** 823–826 (2001).
20. Wopenka, B. & Pasteris, J. D. Structural characterization of kerogens to granulite-facies graphite: applicability of Raman microprobe spectroscopy. *Am. Mineralogist* **78,** 533–557 (1993).
21. Tuinstra, F. & Koenig, J. L. Raman spectrum of graphite. *J. Chem. Phys.* **53,** 1126–1130 (1970).
22. Oehler, J. H. Hydrothermal crystallization of silica gel. *Bull. Geol. Soc. Am.* **87,** 1143–1152 (1976).
23. Baker, R. T. K & Harris, P. in *Chemistry and Physics of Carbon* (ed. Walker, P. L. & Thrower, P. A.) 2–165 (Dekker, New York, 1978).
24. Grotzinger, J. P. & Rothman, D. H. An abiotic model for stromatolite morphogenesis. *Nature* **383,** 423–425 (1996).
25. Westall, F. *et al.* Early Archaean fossil bacteria and biofilms in hydrothermally-influenced sediments from the Barberton greenstone belt, South Africa. *Precambr. Res.* **106,** 93–116 (2001).
26. Holm, N. G. & Charlou, J. L. Initial idicators of abiotic formation of hydrocarbons in the Rainbow ultramafic hydrothermal system, Mid-Atlantic Ridge. *Earth Planet. Sci. Lett.* **191,** 1–8 (2001).
27. Lancet, M. S. & Anders, E. Carbon isotope fractionation in Fischer–Tropsch synthesis and in meteorites. *Science* **170,** 980–982 (1970).
28. Kagi, H. *et al.* Proper understanding of down-shifted Raman spectra of natural graphite: direct estimation of laser-induced rise in sample temperature. *Geochim. Cosmochim. Acta* **58,** 3527–3530 (1994).
29. Matthews, D. E. & Hayes, J. M. Isotope-ratio-monitoring gas chromatography – mass spectrometry. *Anal. Chem.* **50,** 1465–1473 (1978).
30. Clayton, R. N. & Mayeda, T. K. The use of bromine pentafluoride in the extraction of oxygen from oxides and silicates for isotopic analysis. *Geochim. Cosmochim. Acta* **27,** 43–52 (1963).

Supplementary Information accompanies the paper on *Nature*'s website (http://www.nature.com).

Acknowledgements

We thank C. A. Stoakes, A. T. Brasier and D. Huston for assistance with field work; N. Charnley, D. Sansom and A. T. Brasier for laboratory support; the Natural History Museum, London, for the loan of the type slides and re-collected material; R. Buick, J. Farmer, J. P. Grotzinger, A. H. Knoll, E. Nisbet, S. Moorbath, J. W. Schopf and R. E. Summons for comments on earlier versions of the manuscript; and The Royal Society, NASA Astrobiology Institute and The Carnegie Institution of Washington for support. This paper is published by permission of the Director of the Geological Survey of Western Australia.

Competing interests statement

The authors declare that they have no competing financial interests.

Correspondence and requests for materials should be addressed to M.D.B. (e-mail: martinb@earth.ox.ac.uk).